Soil moisture-based study of the variability of dry-wet climate and climate zones in China

LI MingXing[*] & MA ZhuGuo

Key Laboratory of Regional Climate-Environment for East Asia, Institute of Atmospheric Physics, Chinese Academy of Sciences, Beijing 100029, China

An ensemble soil moisture dataset was produced from 11 of 25 global climate model (GCM) simulations for two climate scenarios spanning 1900 to 2099; this dataset was based on an evaluation of the spatial correlation of means and trends in reference to soil moisture simulations conducted using the community land model driven by observed atmospheric forcing. Using the ensemble soil moisture index, we analyzed the dry-wet climate variability and the dynamics of the climate zone boundaries in China over this 199-year period. The results showed that soil moisture increased in the typically arid regions, but with insignificant trends in the humid regions; furthermore, the soil moisture exhibited strong oscillations with significant drought trends in the transition zones between arid and humid regions. The dynamics of climate zone boundaries indicated that the expansion of semiarid regions and the contraction of semi-humid regions are typical characteristics of the dry-wet climate variability for two scenarios in China. During the 20th century, the total area of semiarid regions expanded by 11.5% north of 30°N in China, compared to the average area for 1970–1999, but that of semi-humid regions decreased by approximately 9.8% in comparison to the average for the period of 1970–1999, even though the transfer area of the humid to the semi-humid regions was taken into account. For the 21st century, the dynamics exhibit similar trends of climate boundaries, but with greater intensity.

soil moisture, dry-wet climate, climate zone

Studies on dry-wet climate variability and the boundary dynamics of climate zones are of importance in regard to climate research as well as regional ecological environments and socioeconomic construction. The majority of existing research on dry-wet climate variability is based on precipitation and temperature. For instance, Zhang and Chen [1] calculated the ratio of water demand to precipitation and reported the aridification of semiarid and semi-humid areas, while arid areas began to humidify in the 1970s. The Palmer drought severity index (PDSI) also revealed dry trends in northern China starting in the 1970s and wet trends in northwest China beginning in the 1980s [2]. The variability of observed precipitation suggests a tendency toward more frequent arid events in northeast China as of 1970 [3]. In terms of the boundary dynamics of dry-wet climate zones, it has been reported that the total area of arid regions has shown an increasing trend since the end of the 20th century [4]. An analysis of the decadal variability of climate zone boundaries, according to a dry-wet classification function, indicated that arid areas expanded southeastwards in northern China [5], similar to the trends of expanding arid areas and contracting humid areas found using other indices [6].

The above research on dry-wet climate variability, conducted using mainly precipitation indices, is helpful in furthering our understanding of the characteristics of climate change in China. However, the distribution of precipitation exhibits strong spatial-temporal variability in the terrestrial water cycle due to the impacts of atmosphere, topography, land cover, soil moisture and so on, and such a redistribution

*Corresponding author (email: limx@tea.ac.cn)

directly impacts the land surface conditions. Thus, precipitation indices cannot reflect the effects of climate change on land surface conditions; it can only describe precipitation and temperature aspects. Soil moisture is a key variable in the climate system modulating the water cycle between land and atmosphere. Among early research, Yeh et al. [7] demonstrated the "memory" of soil moisture abnormalities with regard to large-scale precipitation and hydrological processes. Koster et al. [8] reported that eastern China is one of the most sensitive regions with respect to soil moisture responding to climate change. An integrative data analysis by Zuo and Zhang [9] revealed a significant correlation between spring soil moisture and summer precipitation in eastern China. Soil moisture reflects the dry-wet climate variability, and it is also the main water source of many natural ecosystems. Xiao et al. [10] reported that long-term water stress leads to a significant decline in the productivity of an ecosystem. Lovett [11] also noted that soil moisture is the prime stress factor for most middle latitude terrestrial ecosystems. Remote sensing has demonstrated that variability in the vegetation index is sensitive to soil moisture changes in northern China during growing seasons [12]. According to the above research, the evaluation of dry-wet climate conditions, in terms of soil moisture, is significant for climate research as well as eco-environment and agricultural development.

Thus far, there have been many observational studies of soil moisture climate. Wang et al. [13] analyzed the climatic characteristics of soil moisture on various time scales in the west of northwestern China. Zuo and Zhang [14] reported drying trends based on the soil moisture of eastern China in the current spring. Drying has also been reported for northern China in autumn [15]. Additionally, there has been research on the vertical changes of soil moisture and the spatial-temporal relations between precipitation and temperature [16,17]. However, there has been less observational research on the dry-wet climate and boundary dynamics of climate zones on regional scales due to the unavailability of long-term *in situ* soil moisture observations [18]. Furthermore, although remote sensing and monitoring have the advantage of global coverage, the soil moisture data obtained are strongly dependent on the retrieval model used and are constrained by a limited observational depth. Hence, at the present moment, there are many challenges facing observational soil moisture research conducted through remote sensing [19].

With the development of numerical models, models with various physical processes are increasingly employed in soil moisture climate modeling research. Du and Liu [20] used the community land model (CLM) to analyze the potential response of soil moisture variability to global warming. Li et al. [21,22] reported modeling patterns that illustrated the spatial-temporal characteristics of soil moisture variability in China using land and hydrological models driven by observed climate data. Agricultural droughts and their evolution have also been researched using land or hydrology

models in China [23,24]. The above research suggests the practicality of conducting soil moisture climate research using land surface models driven by observational climate data. However, with the limited duration of forcing, soil moisture simulations generally cover less than 60 years in China, which is not long enough to research regional soil moisture climates on long-term scales.

Coupled global climate models (GCMs), which are commonly used for climate change assessment, can produce soil moisture simulations on a 100-year scale [25]. However, simulations based on a single GCM have significant uncertainty [26,27]. The existing research suggests that multiple-model ensemble simulations can significantly reduce the biases of these models and that multiple-model ensemble forecasts are more accurate than those based on a single model [28–30]. In terms of soil moisture research based on ensemble simulations, Guo et al. [31] evaluated ensemble soil moisture data from 17 models and reported that the absolute magnitude, phase and inter-annual variation data were more accurate than those from single model simulations, the finding that is also supported by the ensemble comparisons of soil moisture simulations conducted by Gao and Dirmeyer [32] using multiple models and methods. With regard to the application of ensemble soil moisture, the Global Land-Atmosphere Coupling Experiment studied the regional variability of the feedback of soil moisture to precipitation and temperature using ensemble soil moisture simulations including 16 models [8]. Sheffield and Wood [33] reproduced the large-scale droughts of the 20th century using the ensemble soil moisture simulations of 8 GCMs. An additional analysis of soil moisture simulations from the Intergovernmental Panel on Climate Change (IPCC) also suggested that ensemble soil moisture simulations well represent the basic characteristics of regional climate changes, and then such simulations are frequently used in the research of land surface changes and land-atmosphere interactions [34,35]. Thus, ensemble soil moisture research is a useful approach for representing the dry-wet variability of regional climates and the boundary dynamics of climate zones.

Overall, soil moisture is a key variable representing dry-wet climate variability and the response of land surface processes to climate change, and soil moisture ensemble data obtained from multiple coupled GCMs are capable of capturing the general spatial-temporal patterns of long-term climate variability. Hence, we evaluated the soil moisture simulations of 25 GCMs from IPCC AR4 and, by considering the spatial fidelity, produced a dataset for two scenarios (20C3M and A1B) in China, using 11 GCM simulations that reasonably captured the spatial patterns of means and trends for 30-year soil moisture data. Based on the ensemble soil moisture index, we analyzed the dry-wet variability characteristics of regional climates and the boundary dynamics of climate zones for the period of 1900–2099, for use in ecosystem protection, agriculture and socioeconomy development.

1 Data and methods

1.1 Data

Herein, we used soil moisture simulations from 25 coupled global climate models, which covered two scenarios (20C3M, A1B) and the period of 1900–2099. The description of CO_2 emissions and concentrations for scenarios 20C3M and A1B produced by the IPCC [36] are listed in Table 1, and the details of the GCMs are based on a special report of the IPCC [38] (data downloaded from http://cera-www.dkrz.de). Due to the different land surface models and parameterizations used within various GCMs, the definitions and depths of the soil layers are not consistent. Here, we normalized the soil moisture simulations to the whole soil profile using the simulation minimum and maximum values for all of China. Considering that the standard deviation of the observed volumetric percent soil moisture is approximately 40%, the normalized soil moisture is mapped from 0–40% for comparison, as shown by eq. (1).

$$S_{std} = \frac{S_{grid} - S_{min,cn}}{S_{max,cn} - S_{min,cn}} \times 40.0, \qquad (1)$$

where S_{std} is the normalized grid soil moisture and S_{grid} is the grid soil moisture simulated by the GCMs, representing the water mass of the whole soil profile, given in units of kg m^{-2}. $S_{min,cn}$ and $S_{max,cn}$ are the minimum and maximum simulation values for China, given in the same units as S_{grid}.

The soil moisture data used to assess the simulations of 25 GCMs are produced by the community land model (CLM3.5), which is driven by observation-based climate

data for the period of 1951–2008. The forcing includes precipitation, pressure, temperature, relative humidity, wind speed and radiation (adapted from the dataset of Sheffield et al. [39]); its spatial resolution is 0.5°×0.5°, and the temporal resolution is 3 h (this forcing will be referred to as ObsFC). The model used to produce the historical soil moisture data is CLM3.5 [40,41], and the soil moisture simulation herein is referred to as CLM3.5/ObsFC (Figure 1). For comparison to *in situ* observations, the remote sensing-retrieved soil moisture data and the simulations of the Global Land Data Assimilation System (GLDAS) validate the soil moisture of CLM3.5/ObsFC. The results indicated that the CLM3.5/ObsFC reproduced the historical spatial-temporal characteristics and long-term trends of soil moisture in China. The details of the forcing construction, simulation and validation of soil moisture are given in [42]. In addition, the Palmer drought severity index (PDSI) used herein is that of Dai et al. [43], with global coverage for 2.5°×0.5° latitude-longitude degrees.

1.2 Ensemble method

Soil moisture is primarily controlled by climate change, but it is also closely associated with land cover, topography, soil properties and other regional land surface features. Thus, *in situ* measurements of soil moisture are of significant importance. However, in China, *in situ* measurements of soil moisture began in the 1980s, and measurements were made every 10 d with an observational depth of 0.05–1 m at most sites. The sites were mainly distributed over eastern China. Although these measurements cover the longest

Table 1 Two scenarios produced by the IPCC[a]

Scenario	Duration	CO$_2$ emission	CO$_2$ concentration
20C3M	1850–2000	Peak value, by 2000 ~8 GtC/a	Peak value, by 2000−370 ppm
SRESA1B	2000–2100	Increment, by 2050 ~16 GtC/a, by 2100 ~13 GtC/a	Increment, in 2100−720 ppm

a) From [37]. The common duration for 20C3M is 1900–1999; for A1B, it is 2001–2099.
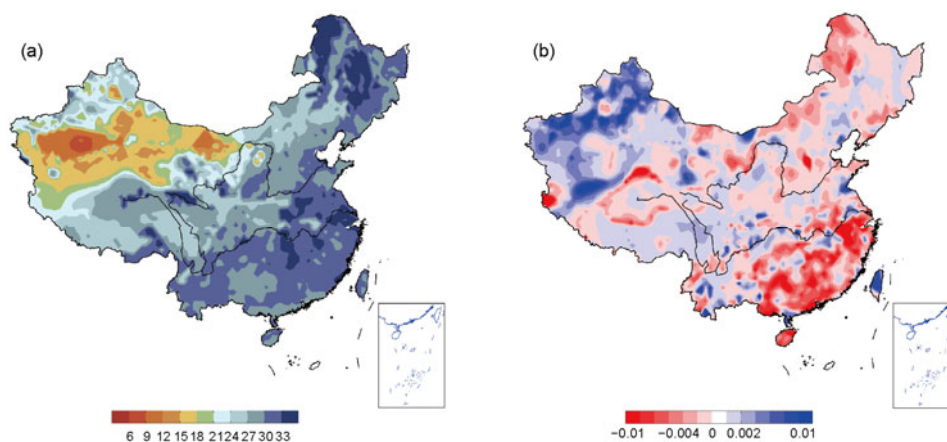

Figure 1   Spatial patterns of means and linear trends for CLM3.5/ObsFC soil moisture for 1970–1999. (a) Soil moisture means (v/v); (b) linear trend means (v v^{-1} a^{-1}).

time span of any observations and include the most extensive spatial coverage in China, the coarse spatial and temporal resolutions make this dataset suitable only for evaluating and validating the simulation for a single site; it is not capable of assessing the long-term trends or spatial patterns of soil moisture simulations for China. Currently, there are no available long-term *in situ* soil moisture observations covering China; thus, we evaluate the soil moisture simulations of the GCMs according to the CLM3.5/ObsFC simulation.

The ensemble soil moisture is produced using the weight-average method given in eq. (2) and the weights accounting for the spatial correlations of means and linear trends between the soil moisture of the GCMs and that of the CLM3.5/ObsFC for 1970–1999. In this way, all errors are independent of the ensemble method, and the variability of the ensemble soil moisture is controlled by the integration of various GCM simulations. In terms of the weight calculation, the spatial correlations of means and linear trends are calculated according to eq. (4) for the GCM simulations and CLM3.5/ObsFC (the correlation coefficients are not shown here). Then, 11 out of the 25 pairs of spatial correlation coefficients were selected to form weights following eq. (3) and to produce the ensemble soil moisture according to eq. (2). Before calculation, the soil moisture data of the GCMs were re-gridded to a 2.5°×2.5° resolution using a bilinear method. The horizontal resolutions and land surface schemes of 11 GCMs are listed in Table 2, and the correlation coefficients and weights are shown in Table 3.

$$S_{em} = \sum_{model=1}^{m} (W_{model} \times S_{std,model}), \qquad (2)$$

where S_{em} is the ensemble soil moisture, and W_{model} is the weight for each GCM, as calculated from eq. (3). m is the number of ensemble GCMs; here, m=11. $S_{std,model}$ is the normalized soil moisture from varying GCMs, calculated from eq. (1).

$$W_{model} = \frac{R_{M,model} \times R_{T,model}}{\sum_{model=1}^{m} (R_{M,model} \times R_{T,model})}, \qquad (3)$$

where $R_{M,model}$ and $R_{T,model}$ are the spatial correlation coefficients of the means and trends for the soil moisture obtained from CLM3.5/ObsFC and the GCMs for the period of 1970–1999, which were calculated using eq. (4).

$$R = \frac{\sum_{grid=1}^{k} W_{grid} \times (S_{gird,GCM} - \overline{S}_{GCM,ave}) \times (S_{grid,CLM} - \overline{S}_{CLM,ave})}{\sqrt{\sum_{grid=1}^{k} W_{grid} \times (S_{grid,GCM} - \overline{S}_{GCM,ave})^2}}$$
$$\times \sqrt{\sum_{grid=1}^{k} W_{grid} \times (S_{grid,CLM} - \overline{S}_{CLM,ave})^2}, \qquad (4)$$

$$W_{grid} = \cos(0.01745329 \times lat), \qquad (5)$$

where $S_{grid,GCM}$ and $S_{grid,CLM}$ are the normalized grid soil moisture values simulated by the GCMs and CLM3.5/ObsFC for 1970–1999, and $\overline{S}_{GCM,ave}$ and $\overline{S}_{CLM,ave}$ are their spatial means over China; k is the grid number in China; W_{grid} is the weight for each area, calculated by eq. (5), where lat is the latitude for each grid.

2 Results

2.1 Comparisons of ensemble soil moisture and CLM3.5/ObsFC

Figure 2 shows a comparison of the spatial patterns of the means and linear trends for the ensemble soil moisture and

Table 2 Description of the coupled global climate models

| Model & year	Sponsor(s) & country	Land resolution	Soil plants routing
CNRM-CM3, 2004	CNRM (Centre National de Recherches Meteorologiques, Meteo-France, France)	64×128	layers, canopy, routing [44–47]
MPI-ECHAM5-MPI-OM, 2005	MPI (Max-Planck-Institute for Meteorology, Germany)	48×96	bucket, canopy, routing [48,49]
DMI-ECHAM5-MPI-OM, 2005	MPI, run 4 from DMI (Danmarks Meteorologiske Institut, Denmark)	96×192	same as above
DMI-ECHAM-C, 2005	MPI, run 3 from DMI (Danmarks Meteorologiske Institut, Denmark)	48×96	same as above
FUB-EGMAM, 2006	FUB IfM (Freie Universitaet Berlin, Institute for Meteorology, Germany)	48×96	bucket, canopy, routing [50,51]
UKMO-HadGEM1, 2004	Hadley Centre for Climate Prediction and Research/Met Office, UK	145×192	layers, canopy, routing [47,52]
IPSL-CM4, 2005	IPSL (Institut Pierre Simon Laplace, France)	143×144	layers, canopy, routing [53]
MIROC3.2 (medres), 2004	CCSR/NIES/FRCGC (Center for Climate System Research, National Institute for Environmental Studies, Frontier Research Center for Global Change, Japan)	320×640	layers, canopy, routing [47]
MRI-CGCM2.3.2, 2003	MRI (Meteorological Research Institute, Japan)	64×128	layers, canopy, routing [54,55]
GISS-ER, 2004	NASA/GISS (Goddard Institute for Space Studies, USA)	46×72	layers, canopy, routing [56,57]
NCAR-CCSM3, 2005	NCAR (National Center for Atmospheric Research, USA)	128×256	layers, canopy, routing [58,59]

Table 3 Spatial correlation coefficients for means and linear trends of the CLM3.5/ObsFC and GCM simulations and weight coefficients[a)]

Model	R for mean	R for trend	Weight
CNRM-CM3	0.37	0.01	0.008
MPI-ECHAM5-MPI-OM	0.82	0.21	0.290
DMI-ECHAM5-MPI-OM	0.76	0.03	0.033
DMI-ECHAM-C	0.82	0.12	0.171
FUB-EGMAM, 2006	0.59	0.19	0.188
UKMO-HadGEM1	0.56	0.02	0.017
IPSL-CM4	0.15	0.21	0.055
MIROC3.2 (medres)	0.82	0.07	0.104
MRI-CGCM2.3.2	0.69	0.07	0.081
GISS-ER	0.44	0.06	0.041
NCAR-CCSM3	0.43	0.02	0.012
ENSEMBLE	0.88	0.31	1.000

a) Duration is 1970–1999; temporal resolution is monthly; *R* is for the spatial coefficient.

CLM3.5/ObsFC (the horizontal resolution is 2.5°×2.5°; the period is 1970–1999). The results suggest that the spatial variability of the ensemble soil moisture reasonably captured the general increasing trends of soil moisture variations from the northwest to the southeast of China, and the dry-wet boundaries are in general agreement. The spatial patterns of CLM3.5/ObsFC and the ensemble soil moisture are consistently characterized by wet trends in the west and dry trends in the east, with especially reasonable agreement between each other in northwest and northern China and south of the Yangtze River. However, in northeast China, both the mean and trends exhibit apparent disagreements, with drier ensemble soil moisture, which mainly resulted from the low horizontal resolution of the GCMs; consequently, the effects do not account for the influence of topography or land cover changes on the variations of soil moisture. In terms of the spatial correlation coefficients for the means and trends (Table 2), both were significant at the $\alpha = 0.001$ level, with 0.88 for the spatial correlation coefficient of the means and 0.31 for that of the linear trends, indicating a better performance in comparison to the simulation variations obtained by single GCMs. The above validation indicated that the ensemble soil moisture well reproduced the spatial distribution and linear trends, which can be further used to research regional climate change.
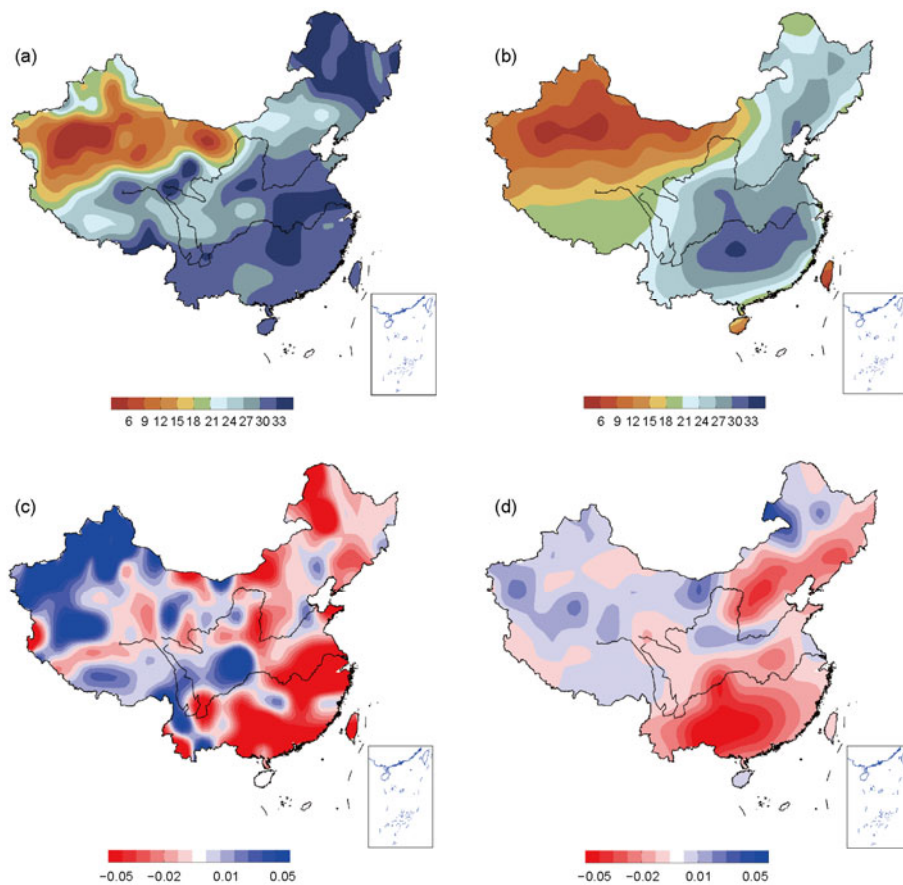
Figure 2 Comparisons of spatial patterns of means and trends of ensemble and CLM3.5/ObsFC soil moisture values for 1970–1999. (a), (b) Spatial patterns of means for CLM3.5/ObsFC and ensemble soil moisture; (c), (d) spatial patterns of linear trends for CLM3.5/ObsFC and ensemble soil moisture (normalized index).

2.2 Spatial characteristics of ensemble soil moisture

Figure 3 shows the spatial distributions of soil moisture and their variances for scenario 20C3M for 1900–1999 and A1B for 2001–2099, which are generally in agreement with the historical simulations for the period of 1951–2008 [22] and which also both agree well with the distributions based on precipitation and temperature [60,61]. The soil moisture decreased gradually from southeast to northwest China, exhibiting high values in the northeast and middle and lower reaches of the Yangtze River. The main dry areas are located in the northwest. The transition zone of the dry-wet regions runs from the northeast to the southwest. In terms of spatial changes of the mean soil moisture, the humid region contracted eastwards during the latter 50 years (1950–1999) in comparison to the former 50 years (1900–1949) of the 20th century, with a decreasing humid area in the middle of the northeast and increasing bilateral dry regions; expanding trends also arose in the northwestern arid and semiarid regions. The variability of soil moisture for the 21st century A1B scenario is characterized by features similar of those of the 20th century, presenting more distinguished southeast-
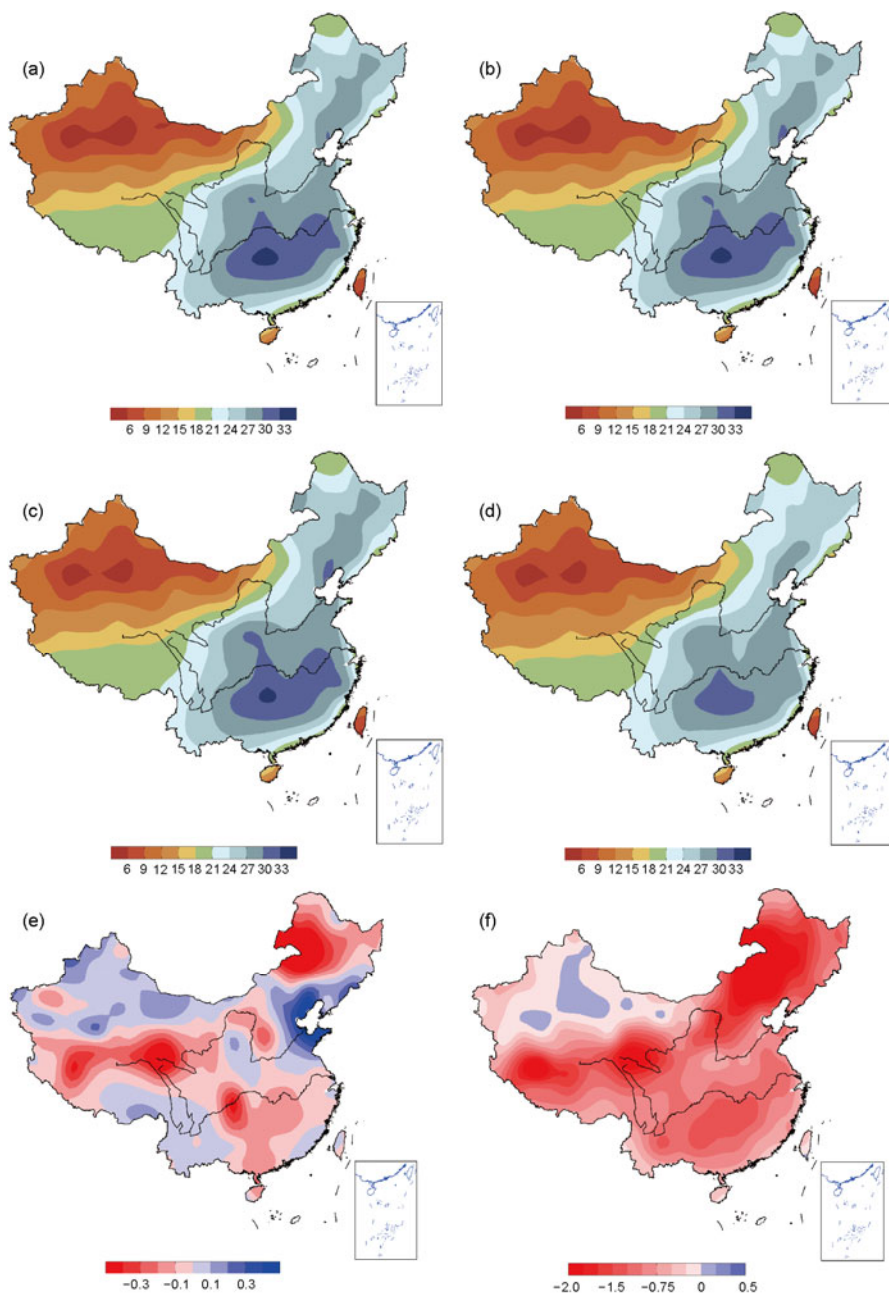

Figure 3 Spatial distributions of ensemble soil moisture and variance. (a)–(d) The periods of 1900–1949, 1950–1999, 2001–2050 and 2051–2099, respectively; (e), (f) the differences between (b) and (a), (d) and (c), respectively.

ward-expanding trends for the dry areas.

The variances between the 20th and the 21st century (Figure 3(e),(f)) suggest that, despite the smaller variation due to dry soil with less precipitation, the mean soil moisture showed rising trends as of the 1950s. The humid area showed significant contraction southeastwards, especially during the 21st century, which resulted in the southeast expansion of dry-wet transition zones. For 1900–1999, the soil moisture changed significantly in the northeast, with decreasing humid areas and relatively smaller changes in the northwest. On the other hand, for 2001–2099, the transition zones expanded approximately 1° to 5° longitude in North

China and Northeast China, along with an obvious contraction of humid regions in eastern China.

2.3 Spatial patterns of linear trends for ensemble soil moisture

The spatial patterns of the linear trends of the ensemble soil moisture (Figure 4) illustrate that the soil moisture level decreased during 1900–1999 in Northeast China and North China, the northern part of the Qinghai-Tibetan Plateau and the Yangtze River basin, while increasing in the northwest and southern parts of North China and the Yellow River
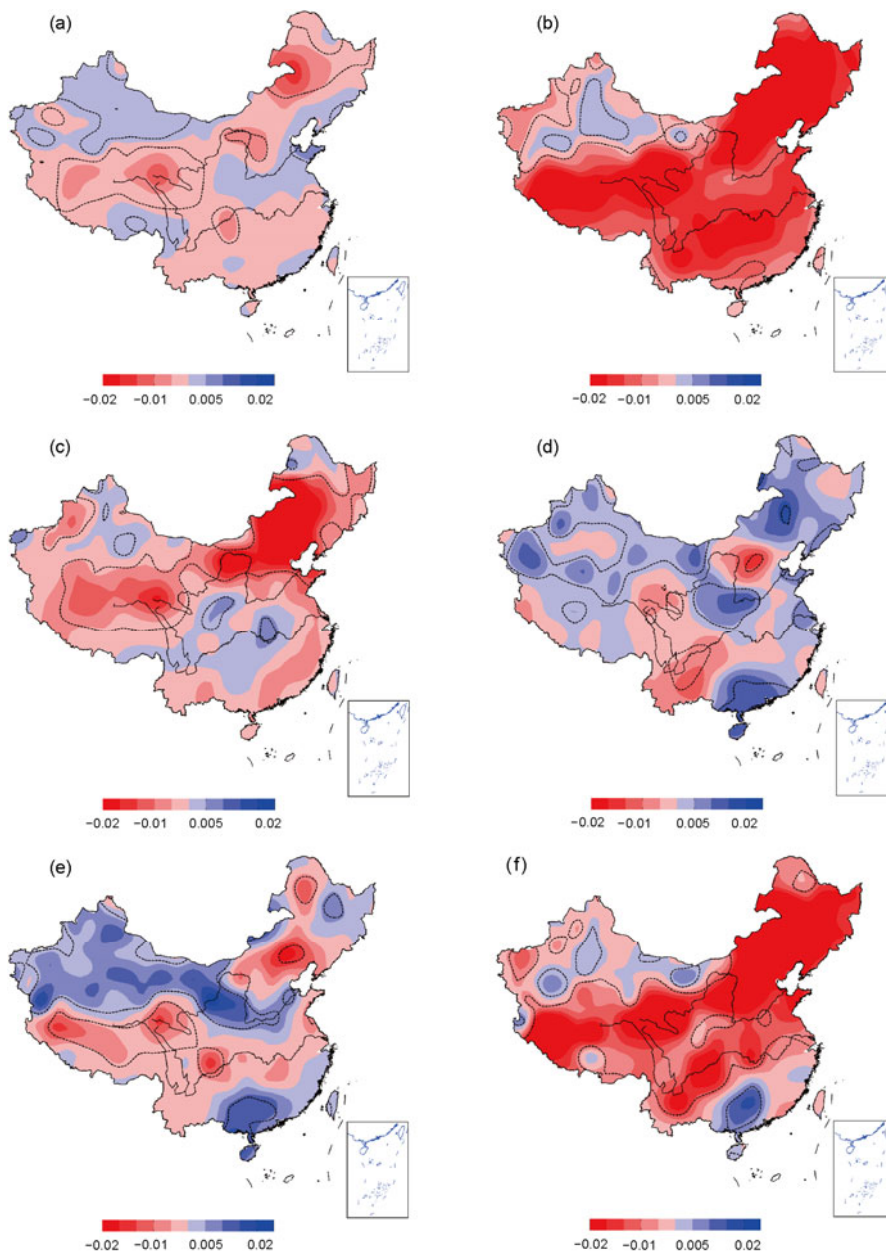

Figure 4   Spatial patterns of the linear trends of ensemble soil moisture. (a), (b) 1900–1999, 2001–2099; (c), (d) 1901–1950, 1951–1999, (e), (f) 2001–2050, 2051–2099. Black dot line indicates significance at α=0.05 level.

basin. As for the linear trends, the soil moisture presented increasing trends in the typically arid regions of northwestern China for the 20th century, while developing dry trends in the semiarid regions. In the 21st century scenario A1B, the soil moisture level decreased not only in the typically semiarid regions, but also throughout most of China, except for the northwestern area, in which the soil moisture increased. On the other hand, the 50-year trends show that the soil moisture decreased throughout most of China during the first 50 years of the 20th century, with significant trends in Northeast China and North China and the Qinghai-Tibetan Plateau; yet, increasing soil moisture trends were exhibited in the northwest and in parts of the Yangtze River basin. However, the soil moisture presented increasing trends throughout most of China during the latter 50 years, with expanded humidifying areas in Northwest China and Northeast China and the south of the Yangtze River. In the 21st century, the spatial features of the linear trends for the former 50 years generally agree with those of the latter 50 years of the 20th century, with only an inversion to the aridification occurring in the south of the Qinghai-Tibetan Plateau. Additionally, the variations in soil moisture over the latter 50 years of the 21st century are similar to those of the former 50 years of the 20th century, but with much greater intensity.

The temporal evolution of the spatial patterns of the linear trends was characterized by decadal transformations (not shown in the figure) or longer temporal cycles (exhibiting 30- to 60-year periods (Figure 1)), which often occurred in the dry-wet transition zone with relatively high frequencies.

To describe the regional features of the temporal evolution of the ensemble soil moisture, here we partitioned the entire domain into six regions, following the linear trends. Figure 5 shows the 11-year running mean of the soil moisture for 1900–2099. The soil moisture level increased in the northwest from 1900 to 1999, but decreased with various trends in the other five regions, particularly in the Qinghai-Tibetan Plateau and Northeast China. The linear trends changed from aridification to humidifying trends in North China and Northeast China in the 1950s, along with aridification trends throughout the period. For scenario A1B, the soil moisture presents decreasing trends as of the 2040s, with regionally different intensities. The oscillations of the running means removed the linear trends, implying that the soil moisture fluctuates much more in the dry-wet transition zone than in typically arid or humid regions, and this behavior grew stronger with time. The correlation coefficients (not shown) of the regional means of soil moisture also presented a relatively high consistency of soil moisture variations in the dry-wet transition zone.

The correlation of the soil moisture with precipitation and temperature changed regionally (Figure 5), especially in scenario A1B. Overall, the soil moisture decreased with rising temperatures, although the ranges varied for the different regions. The precipitation was higher in Northeast China and Northwest China and in the Yangtze River basin, but was lower in northern China and the Qinghai-Tibetan and Yunnan-Guizhou plateaus, exhibiting values 3 orders of magnitude lower in the Qinghai-Tibetan Plateau than those of the other regions. The soil moisture showed a negative correlation with temperature in the northeast and northwest (correlation coefficients of -0.462 and -0.469, respectively, significant at $\alpha = 0.01$ level), which implies that the soil moisture decreases with increasing temperature due to evapotranspiration, even though the precipitation presents increasing trends. However, the combined effects of rising temperatures and decreasing precipitation led to dry soil moisture trends in northern China and the Qinghai-Tibetan and Yunnan-Guizhou plateaus.

A comparison of the soil moisture and the PDSI showed that their long-term variation trends are almost opposite each other, except in northern China and the Yangtze River basin, a trend that is associated with the difference between the definitions of soil moisture and the PDSI. Dai et al. [43] noted that the PDSI cannot completely represent soil moisture variations. Currently, research observations have a 10-day resolution, and measurements are suspended when precipitation occurs or when the sampled soil freezes. Therefore, the monthly series of the ensemble soil moisture cannot be evaluated by using observations. Considering the fidelity of the spatial-temporal variations of the CLM3.5/ObsFC soil moisture compared to the observations on various time scales (for example, the correlation coefficient is 0.84 for CLM3.5/ObsFC and observations in northeast China for 1990–2000, showing decreasing trends) [22], Figure 6 shows a comparison of the CLM3.5/ObsFC results and the ensemble soil moisture series, indicating that the variations agree well with each other on the decadal scale, especially over the latter 20 years. The results suggest that this is a practical approach for analyzing the dry-wet conditions and boundary dynamics of climate zones on a decadal scale.

2.4 Dry-wet climate zones and boundary dynamics

The existing research on climate zone divisions are commonly based on dry-wet indices calculated using observed precipitation, temperature or grid data, such as that of the Climate Research Unit [5,62,63], involving the main factors controlling regional dry-wet changes and reflecting the general characteristics of regional climates. Therefore, using soil moisture criteria, we divided the domain into five dry-wet climate regions, according to existing divisions (Figure 7). Compared with existing divisions, they agree well in the typically arid, extreme arid and humid climate zones. In the semi-arid and semi-humid regions, various indices presented differences due to the increasing weights of the effects of topography, soil properties, land cover and other terrestrial factors governing soil moisture variations [5,62].

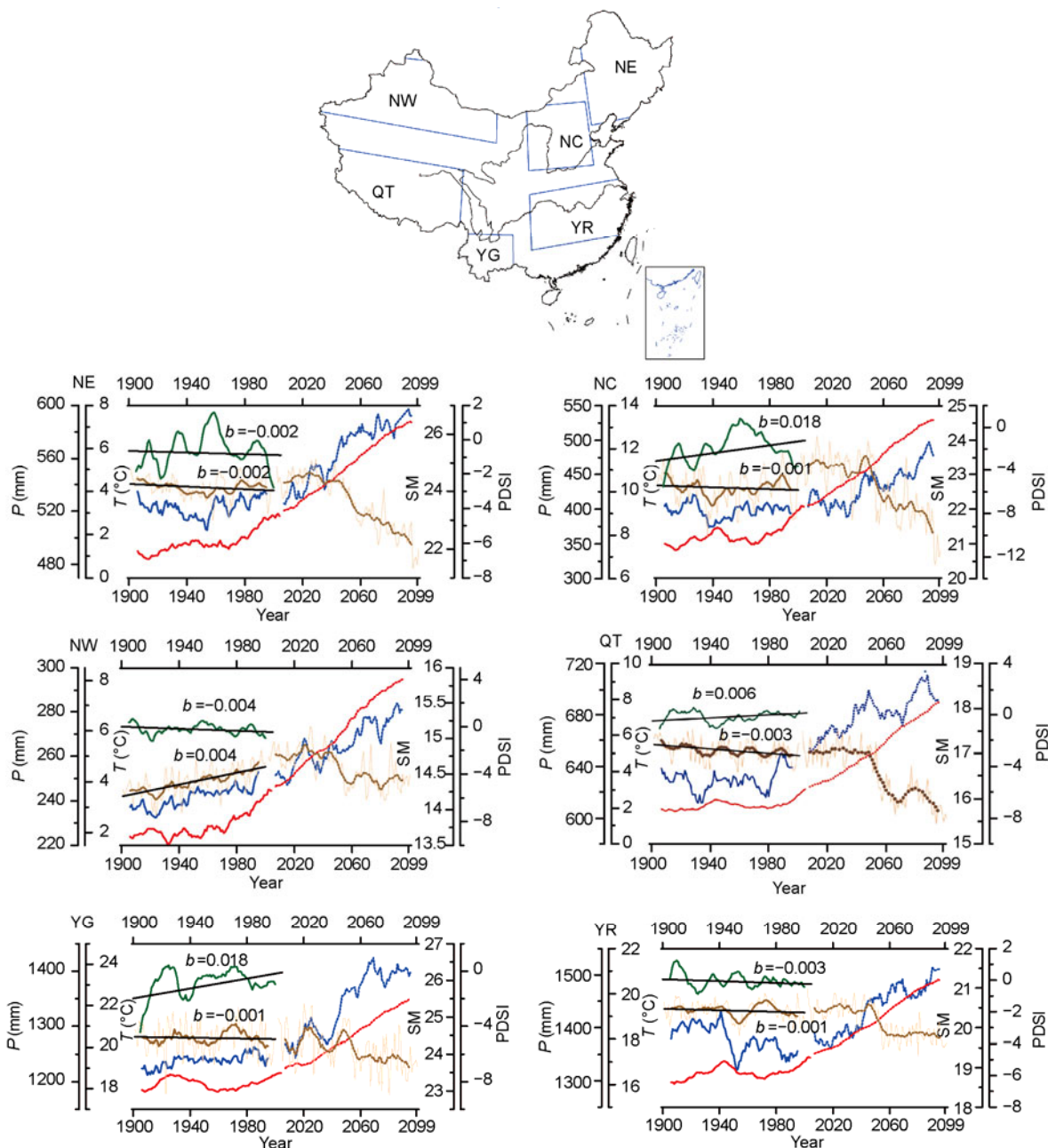Figure 8 shows the boundary dynamics of 5-year means

Figure 5 Comparisons between regional means of ensemble soil moisture results and precipitation, temperature and PDSI. Blue line, precipitation (*P*); red line, temperature (*T*); brown line, normalized soil moisture (SM); green line, PDSI; solid line, scenario 20C3M; dotted line, scenario A1B; black straight line, regression linear trends; *b* is the coefficient of the linear trends. NE, Northeast China; NC, North China; NW, Northwest China; QT, Qinghai-Tibetan Plateau; YG, Yunan-Guizhou Plateau; YR, Yangtze River basin.

for 1900–2099, which suggest that the semiarid and semi-humid regions changed during the 20th century in the 20C3M scenario, with southeastward expansion in the semi-arid regions and eastward contraction in the semi-humid regions. During 2001–2099 in scenario A1B, the boundary dynamics are similar to the trends for 20C3M, but with much stronger variations. In addition, the area of the humid region decreased significantly, a trend that is closely associated with decreasing precipitation and rising temperatures. However, the area of the extreme arid regions changed little

in the northwest and even decreased with increasing precipitation.

The spatial patterns of the standard deviations for soil moisture imply strong fluctuations in the dry-wet transition zone (Figure 9). In scenario 20C3M, the fluctuations were strong in the arid and semiarid regions, such as northeast and northern China; this result is obvious in the typically semiarid regions for scenario A1B. Therefore, the soil moisture oscillated strongly in the dry-wet transition zone for both scenarios 20C3M and A1B, and the effects on the
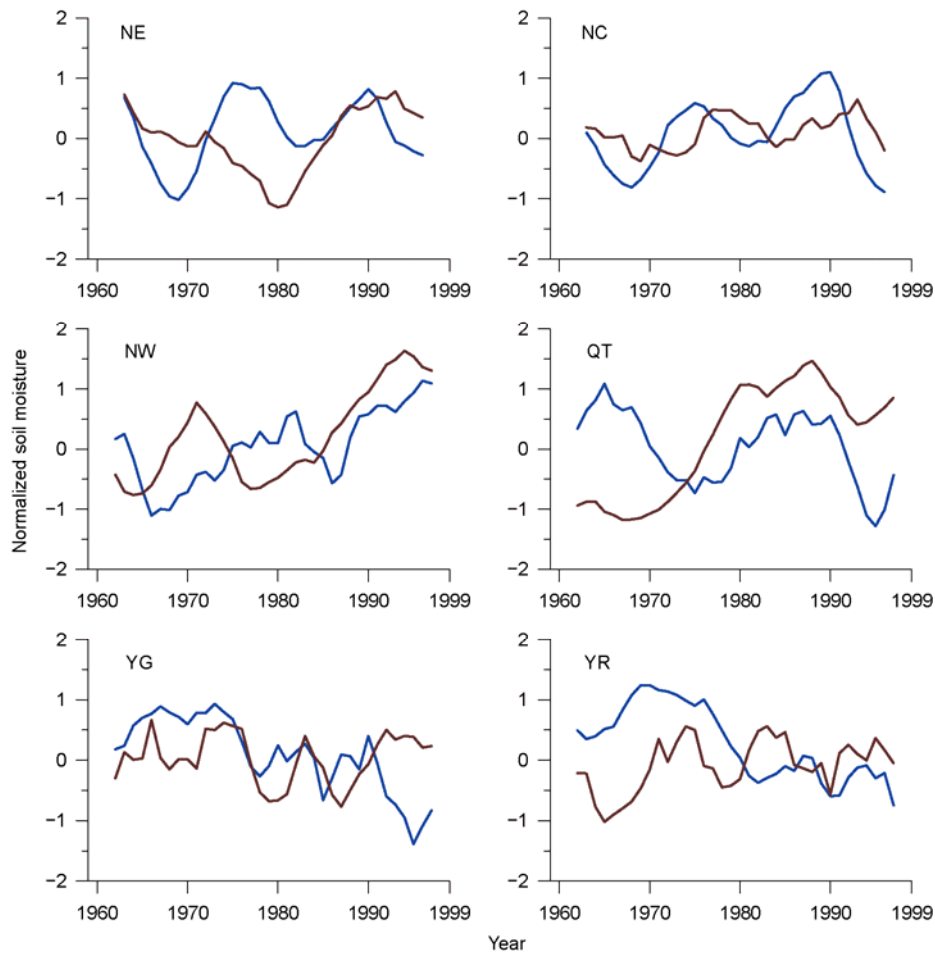
Figure 6 Comparisons between ensemble soil moisture and CLM3.5/ObsFC. Each curve represents the 7-year running mean for 1960–1999; the blue line is CLM3.5/ObsFC, and the brown line is ensemble soil moisture.
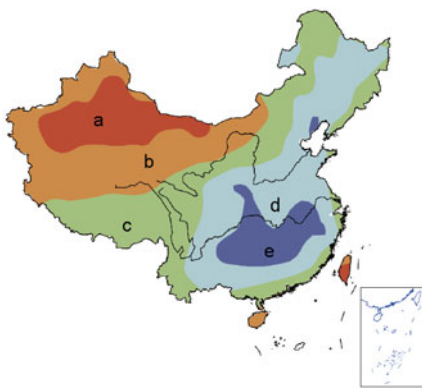

Figure 7 Divisions of dry-wet climate zones based on ensemble soil moisture results for 1970–1999. (a) Extreme arid region; (b) arid region; (c) semiarid region; (d) semi-humid region; (e) humid region.

ecosystem require further study.

With regard to the features of the boundary dynamics, the boundary moves in an east-west direction for the semi-arid and semi-humid regions along the latitude line of 45°N; the other boundaries move in a south-north direction along the longitude lines of 111° and 115°E, respectively, as

shown in Figure 10. This result suggests that the boundary movements were characterized by periodic swings, with eastward expansions before 1940 and westward recessions after 1940. The 1980s represent the most significant period of eastward expansion of the semiarid and semi-humid regions during the 20th century. The boundary dynamics reproduced the well-known drought events throughout the 20th century, such as the national droughts of 1928–1929 and 1941–1943 and the severe northern drought of 1997–2001 [64]. The boundary movements present approximately 8-year and 16-year periods during 2001–2099 in scenario A1B, reaching the receding phrase of a 16-year period during the period of 2001–2015 and then gradually expanding eastwards. The boundary dynamics of the semiarid and semi-humid regions are highly synchronized, which indicates that the aridification developed rapidly around the 1940s, with strong southward boundary expansion, while the climate is in the most humid phrase around the 1980s, with the most significant northward boundary contraction. Figure 10(b) shows the larger amplitude of the semiarid semi-humid boundary in comparison to that of the arid and semi-arid climate zones, indicating that the water balance
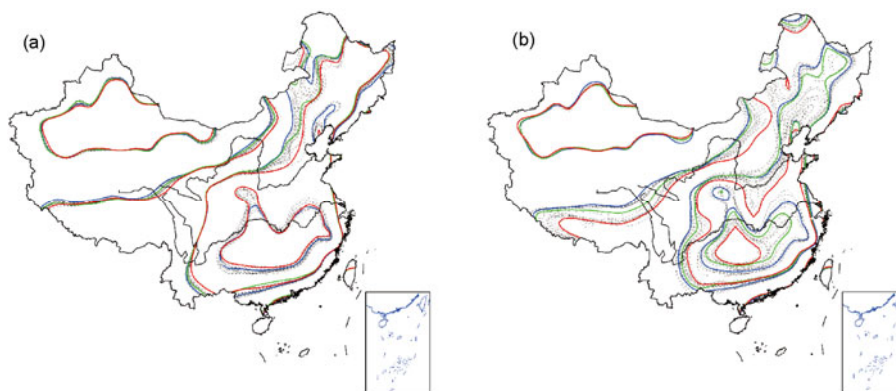
Figure 8   Boundary dynamics of 5-year means based on ensemble soil moisture. (a) 1900–1999; (b) 2001–2099. The blue lines denote means for 1900–1904 (a) and (2001–2005) (b), green ones denote means for 1950–1954 (a) and 2050–2054 (b), and the red lines denote means for 1995–1999 (a) and 2095–2099.
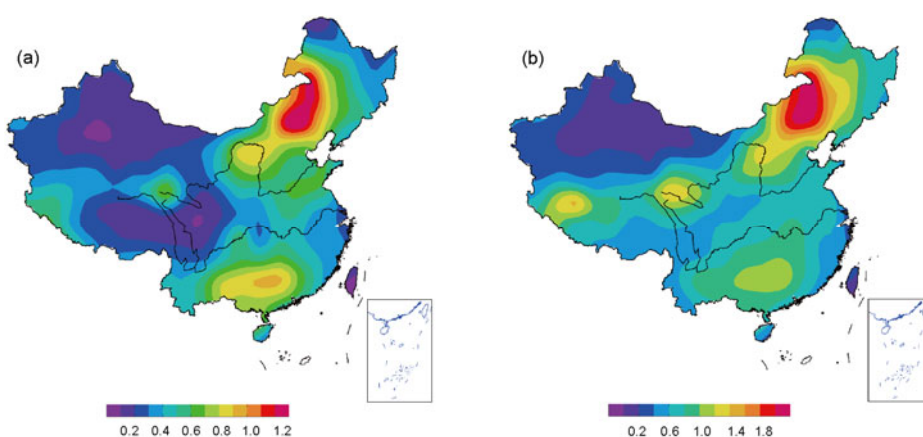

Figure 9   Spatial patterns of standard deviations for ensemble soil moisture. (a) 1900–1999; (b) 2001–2099.
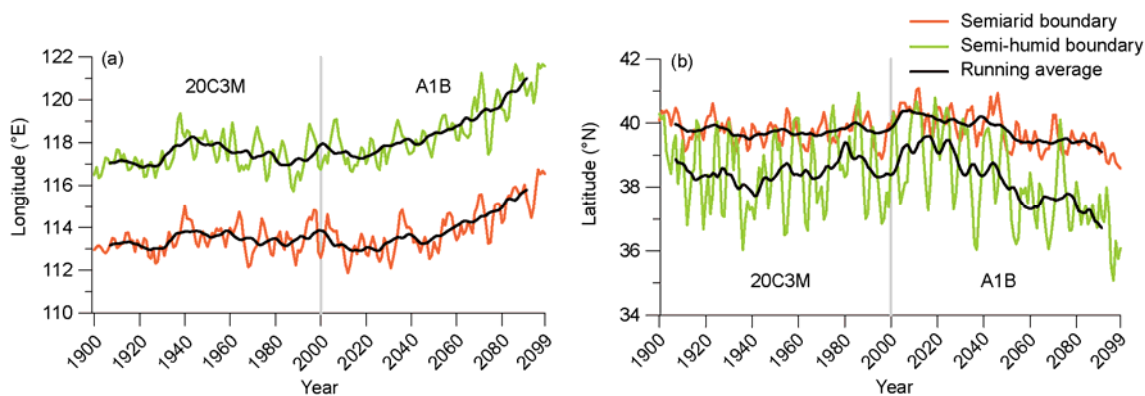

Figure 10   Dynamics of boundaries between arid, semiarid and semi-humid climate zones. (a) The movements of boundaries in an east-west direction along the latitude line of 43°N; (b) in a south-north direction along the longitude lines of 111° and 115°E, respectively.

fluctuated intensively in the transition zone. A wavelet analysis (Figure 11) also implied that the movements of dry-wet boundaries have shorter 2- to 4-year periods, as well as 8-year, 16-year, 30-year and 60-year periods. All of the above analyses mainly focused on the typically semi-arid and semi-humid regions north of 35°N and east of 100°E.

The boundary movements of various climate zones led to areas of climate zone variation. Figure 12 shows the area variations of the semiarid, semi-humid and humid regions for 1900–1999 (scenario 20C3M) and 2001–2099 (A1B). The boundary movements caused the arid region area to expand southeastwards by 140000 km^2 from 1900–1904 to 1995–1999, up to 4.4% of the average for 1970–1999. The
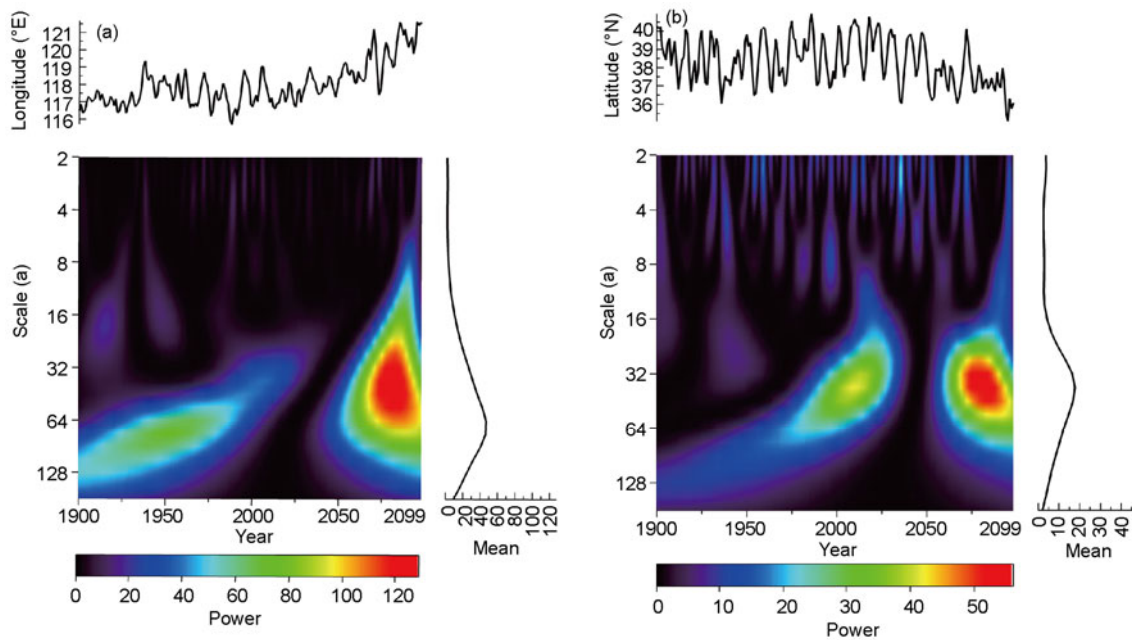
Figure 11 Wavelet analyses of boundary dynamics with time. (a) The boundary between arid and semiarid regions; (b) that between semiarid and semi-humid regions.
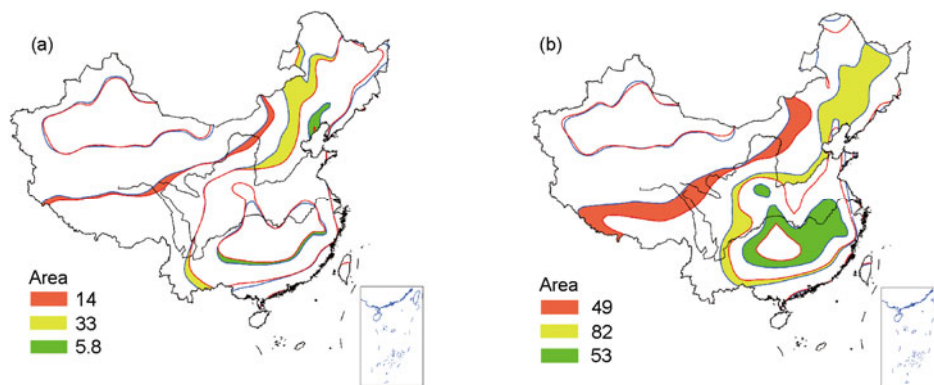

Figure 12 Area variations of dry-wet climate zones. (a) The mean for 1900–1999; (b) the mean for 2001–2099 (10^4 km^2).

semi-arid region increased by 300000 km^2 north of 30°N, equaling 11.5% of the average for the period of 1970–1999, while the contraction of the semi-humid region is approximately 9.8% of the average for 1970 to 1999. Figure 12(b) shows that the arid region expanded southeastwards by approximately 490000 km^2 throughout the 21st century, up to 15.4% of the average for 1970–1999, along with an 820000-km^2 eastward expansion of the semi-arid region, corresponding to approximately 31.5% of the 1970–1999 mean. However, the humid region contracted 70.4% of the mean for 1970–1999, approximately 530000 km^2. In scenario 20C3M, the dry-wet climate zone variations and resulting area changes mostly occurred in the semi-arid and semi-humid regions north of 35°N and east of 105°E; with the exception of these regions, in scenario A1B, the development of aridification also impacted the regions south of 35°N, especially the humid region.

3 Discussion and conclusion

Based on the soil moisture simulation of CLM3.5 with observational forcing, we evaluated the soil moisture simulations obtained by GCMs by calculating spatial correlation coefficients and also produced ensemble soil moisture data according to the spatial correlation for two scenarios (20C3M and A1B) from 1900 to 2099. We then analyzed the spatial-temporal characteristics of dry-wet climate changes. By dividing the dry-wet climate zones using soil moisture criteria, we analyzed the spatial-temporal features of dry-wet transition zone evolution and resulting area changes.

In comparing the ensemble soil moisture results to single GCM simulations, it was found that both the averaged spatial patterns for 1970–1999 and the 30-year linear trends

correlated with CLM3.5/ObsFC simulations with greatly enhanced spatial correlation coefficients. The results provide support for use of the weight ensemble method in multiple-model ensemble studies of soil moisture. The ensemble soil moisture results presented a gradual increase from northwest to southeast China and extremely low values in the sandy regions of Xinjiang and west of Inner Mongolia; the main humid regions are located in northeastern China and the Yangtze River basin. The transition zone includes the areas between arid and humid regions from Northeast China to Southwest China. In terms of long-term linear trends, the soil moisture tended to increase in the northwest, while decreasing in northeast and northern China; in general, humidification was observed in the southern area of the Yangtze River, but with frequent conversions between aridification and humidification. On the other hand, the deviation of the ensemble soil moisture from the CLM3.5/ObsFC results is relatively high; therefore, ensemble research requires further validation.

By dividing the dry-wet climate zones based on ensemble soil moisture levels, we analyzed the features of the boundary dynamics and resulting area changes of various climate zones. The results revealed southeastward expansions of semiarid and semi-humid climate zones in the 20th century, especially in northern China, with a more significant tendency in the 21st century for scenario A1B. The quantitative estimations of the area changes of various climate zones have uncertainty due to the biases of the GCMs and land surface schedules; however, the qualitative results agreed well with existing research, suggesting that the dry-wet transition zone is sensitive to climate change and that aridification development and its effects on ecosystems and socio-economies deserve further research.

1   Zhang Q Y, Chen L T. Variations of dryness and wetness in China during 1951–1980 (in Chinese). Chin J Atmos Sci, 1991, 5: 72–81

2   Su M F, Wang H J. Relationship and its instability of ENSO — Chinese variations in droughts and wet spells. Sci China Ser D-Earth Sci, 2007, 50: 145–152

3   Bordi I, Fraedrich K, Jiang J M, et al. Spatio-temporal variability of dry and wet periods in eastern China. Theor Appl Climatol, 2004, 79: 81–91

4   Yang J P, Ding Y J, Chen R S, et al. The interdecadal fluctuation of dry and wet climate boundaries in China in recent 50 years (in Chinese). Acta Geogr Sin, 2002, 6: 655–661

5   Ma Z G, Fu C B. Decadal variations of and and semiarid boundary in China (in Chinese). Chin J Geophys, 2005, 48: 519–525

6   Liu B, Ma Z G. Area change of dry and wet regions in China in the past 45 years (in Chinese). Arid Land Geogr, 2007, 1: 7–15

7   Yeh T C, Wetherald R T, Manabe S. The effect of soil-moisture on the short-term climate and hydrology change—A numerical experiment. Mon Weather Rev, 1984, 112: 474–490

8   Koster R D, Dirmeyer P A, Guo Z C, et al. Regions of strong coupling between soil moisture and precipitation. Science, 2004, 305: 1138–1140

9   Zuo Z Y, Zhang R H. The spring soil moisture and the summer rainfall in eastern China. Chin Sci Bull, 2007, 52: 3310–3312

10 Xiao J F, Zhuang Q L, Liang E Y, et al. Twentieth-century droughts and their impacts on terrestrial carbon cycling in China. Earth Int, 2009, 13: 1–31

11 Lovett R A. Global warming-rain might be leading carbon sink factor. Science, 2002, 296: 1787–1787

12 Zhang Q, Xiao F J, Niu H S, et al. Analysis of vegetation index sensitivity to soil moisture in Northern China (in Chinese). Chin J Ecol, 2005, 7: 715–718

13 Wang L, Wen J, Wei Z G, et al. Soil moisture over the west of northwest china and its response to climate (in Chinese). Plateau Meteorol, 2008, 6: 1257–1266

14 Zuo Z Y, Zhang R H. Temporal and spatial features of the soil moisture in boreal spring in eastern China. Sci China Ser D-Earth Sci, 2009, 52: 269–278

15 Guo W D, Ma Z G, Yao Y H. Regional characteristics of soil moisture evolution in Northern China over recent 50 years (in Chinese). Acta Geogr Sin, 2003, 58: 83–90

16 Sun C H, Li W J, Zhang Z Q, et al. Impact of huaihe river basin soil temperature and humidity abnormality in pre winter and springtime on the anomalous summer rainfall and its application (in Chinese). Acta Meteorol Sin, 2005, 1: 115–122

17 Zhang X Z, Wu X Y, He J H. Vertical character of soil moisture in China (in Chinese). Acta Meteorol Sin, 2004, 62: 51–61

18 Robock A, Vinnikov K Y, Srinivasan G, et al. The global soil moisture data bank. Bull Amer Meteorol Soc, 2000, 81: 1281–1299

19 Kerr Y H. Soil moisture from space: Where are we?. Hydrogeol J, 2007, 15: 117–120

20 Du C L, Liu X D. CLM3-simulated chinese soil moisture during 1979–2003 and its possible response to global warming (in Chinese). Plateau Meteorol, 2008, 3: 463–473

21 Li M X, Ma Z G, Du J W. Regional soil moisture simulation for Shaanxi province using SWAT model validation and trend analysis. Sci China-Earth Sci, 2010, 53: 575–590

22 Li M X, Ma Z G, Niu G Y. Modeling spatial and temporal variations in soil moisture in China. Chin Sci Bull, 2011, 56: 1809–1820

23 Wu Z Y, Lu G H, Wen L, et al. Reconstructing and analyzing China's fifty-nine year (1951–2009) drought history using hydrological model simulation. Hydrol Earth Syst Sci, 2011, 15: 2881–2894

24 Wang A H, Lettenmaier D P, Sheffield J. Soil moisture drought in China, 1950–2006. J Clim, 2010, 24: 3257–3271

25 Meehl G A, Covey C, Delworth T, et al. The WCRP CMIP3 multimodel dataset—A new era in climate change research. Bull Amer Meteorol Soc, 2007, 88: 1383–1394

26 Robock A, Schlosser C A, Vinnikov K Y, et al. Evaluation of the AMIP soil moisture simulations. Glob Planet Change, 1998, 19: 181–208

27 Li H B, Robock A, Wild M. Evaluation of intergovernmental panel on climate change fourth assessment soil moisture simulations for the second half of the twentieth century. J Geophys Res, 2007, 112, doi: 10.1029/2006JD007455

28 Krishnamurti T N, Kishtawal C M, Larow T E, et al. Improved weather and seasonal climate forecasts from multimodel superensemble. Science, 1999, 285: 1548–1550

29 Barnston A G, Mason S J, Goddard L, et al. Multimodel ensembling in seasonal climate forecasting at IRI. Bull Amer Meteorol Soc, 2003, 84: 1783–1796

30 Palmer T N, Alessandri A, Andersen U, et al. Development of a european multimodel ensemble system for seasonal-to-interannual prediction (DEMETER). Bull Amer Meteorol Soc, 2004, 85: 853–872

31 Guo Z C, Dirmeyer P A, Gao X, et al. Improving the quality of simulated soil moisture with a multi-model ensemble approach. Quart J Res Meteorol Soc, 2007, 133: 731–747

32 Gao X, Dirmeyer P A. A multimodel analysis, validation, and

transferability study of global soil wetness products. J Hydrometeorol, 2006, 7: 1218–1236

33 Sheffield J, Wood E F. Projected changes in drought occurrence under future global warming from multi-model, multi-scenario, IPCC AR4 simulations. Clim Dyn, 2008, 31: 79–105

34 Wetherald R T, Manabe S. Simulation of hydrologic changes associated with global warming. J Geophys Res, 2002, 107, doi: 10.1029/2001 JD001195

35 Wang G L. Agricultural drought in a future climate: Results from 15 global climate models participating in the IPCC 4th assessment. Clim Dyn, 2005, 25: 739–753

36 Nakicenovic N, Alcamo J, Davis G, et al. Special Report on Emissions Scenarios: A Special Report of Working Group III of the Intergovernmental Panel on Climate Change. New York: Cambridge University Press, 2000. 6–10

37 Frei A, Gong G. Decadal to century scale trends in north american snow extent in coupled atmosphere-ocean general circulation models. Geophys Res Lett, 2005, 32, doi: 10.1029/2005GL023394

38 Randall D A, Wood R A, Bony S, et al. Cilmate models and their evaluation. In: Climate change 2007: The physical science basis. Contribution of Working Group I to the Fourth Assessment Report of the Intergovernmental Panel on Climate Change. New York: Cambridge University Press, 2007. 597–599

39 Sheffield J, Goteti G, Wood E F. Development of a 50-yr high-resolution global dataset of meteorological forcings for land surface modeling. J Clim, 2006, 19: 3088–3111

40 Dai Y J, Zeng X B, Dickinson R E, et al. The common land model. Bull Amer Meteorol Soc, 2003, 84: 1013–1023

41 Oleson K W, Niu G Y, Yang Z L, et al. Improvements to the Community Land Model and their impact on the hydrological cycle. J Geophys Res, 2008, 113, doi: 10.1029/2007JG000563

42 Li M X, Ma Z G. Comparisons of simulations of soil moisture variations in the Yellow River basin driven by various atmospheric forcing data sets. Adv Atmos Sci, 2010, 27: 1289–1302

43 Dai A G, Trenberth K E, Qian T T. A global dataset of palmer drought severity index for 1870–2002: Relationship with soil moisture and effects of surface warming. J Hydrometeorol, 2004, 5: 1117–1130

44 Mahfouf J F, Manzi A O, Noilhan J, et al. The land-surface scheme ISBA within the meteo-france climate model ARPEGE. Part I. implementation and preliminary results. J Clim, 1995, 8: 2039–2057

45 Douville H, Royer J F, Mahfouf J F. A new snow parameterization for the meteo-france climate model. Part I. Validation in stand-alone experiments. Clim Dyn, 1995, 12: 21–35

46 Douville H, Royer J F, Mahfouf J F. A new snow parameterization for the meteo-france climate model. Part II. validation in a 3-D GCM experiment. Clim Dyn, 1995, 12: 37–52

47 Oki T, Sud Y C. Design of Total Runoff Integrating Pathways (TRIP) — A global river channel network. Earth Int, 1998, 2:1–37

48 Hagemann S, Gates L D. Validation of the hydrological cycle of ECMWF and NCEP reanalyses using the MPI hydrological discharge model. J Geophys Res, 2001, 106: 1503–1510

49 Schulz J P, Dumenil L, Polcher J. On the land surface-atmosphere coupling and its impact in a single-column atmospheric model. J Appl Meteorol, 2001, 40: 642–663

50 Roeckner E, Brokopf R, Esch M, et al. Sensitivity of simulated climate to horizontal and vertical resolution in the ECHAM5 atmosphere model. J Clim, 2006, 19: 3771–3791

51 Roeckner E, Bäuml G, Bonaventura L. The atmospheric general circulation model ECHAM5: Part I: model description. Max-Planck-Institut für Meteorologie, Bundesstrasse 55 D-20146 Hamburg Germany, 2003. 35–43

52 Essery R, Pomeroy J, Parviainen J, et al. Sublimation of snow from coniferous forests in a climate model. J Clim, 2003, 16: 1855–1864

53 Krinner G, Viovy N, De Noblet-Ducoudre N, et al. A dynamic global vegetation model for studies of the coupled atmosphere-biosphere system. Glob Biogeochem Cycle, 2005, 19, doi: 10.1029/2003GB 002199

54 Sellers P J, Mintz Y, Sud Y C, et al. A simple biosphere model (SIB) for use within general circulation models. J Atmos Sci, 1986, 43: 505–531

55 Sato N, Sellers P J, Randall D A, et al. Effects of implementing the simple biosphere model in a general-circulation model. J Atmos Sci, 1989, 46: 2757–2782

56 Abramopoulos F, Rosenzweig C, Choudhury B. Improved ground hydrology calculations for Global Climate Models (GCMs): Soil water movement and evapotranspiration. J Clim, 1988, 1: 921–941

57 Miller J R, Russell G L, Caliri G. Continental-scale river flow in climate models. J Clim, 1994, 7: 914–928

58 Oleson K W, Bonan G B, Feddema J. Effects of white roofs on urban temperature in a global climate model. Geophys Res Lett, 2010, 37, doi: 10.1029/2009GL042194

59 Oleson K W, Niu G Y, Yang Z L, et al. Improvements to the community land model and their impact on the hydrological cycle. J Geophys Res, 2008, 113, doi: 10.1029/2007JG000563

60 Ma Z G, Fu C B. Some evidence of drying trend over northern China from 1951 to 2004. Chin Sci Bull, 2006, 51: 2913–2925

61 Ma Z, Dan L, Hu Y. The extreme dry/wet events in northern china during the recent 100 years. J Geogr Sci, 2004, 14: 275–281

62 Yang J P, Ding Y J, Chen R S, et al. Fluctuations of the semi-arid zone in china, and consequences for society. Clim Change, 2005, 72: 171–188

63 Mao F, Sun H, Yang H L. Research progress in dry/wet climate zoning (in Chinese). Prog Geogr, 2011, 30: 17–26

64 Zhang Q, Pan X B, Ma Z G, et al. Drought. Beijing: China Meteorological Press, 2009. 192–195